Journal Pre-proofs

Oxygen vacancy-enriched $V_2O_5 \cdot nH_2O$ nanofibers ink for universal substrates-tolerant and multi means-integratable NH_3 sensing

Xiaxia Xing, Xinhua Zhao, Zhenxu Li, Lingling Du, Chen Wang, Dongliang Feng, Dongsheng Geng, Robert Bogdanowicz, Dachi Yang

PII: S1385-8947(23)05964-8
DOI: https://doi.org/10.1016/j.cej.2023.147233
Reference: CEJ 147233

To appear in: *Chemical Engineering Journal*

Received Date: 16 July 2023
Revised Date: 22 September 2023
Accepted Date: 7 November 2023

Please cite this article as: X. Xing, X. Zhao, Z. Li, L. Du, C. Wang, D. Feng, D. Geng, R. Bogdanowicz, D. Yang, Oxygen vacancy-enriched $V_2O_5 \cdot nH_2O$ nanofibers ink for universal substrates-tolerant and multi means-integratable NH_3 sensing, *Chemical Engineering Journal* (2023), doi: https://doi.org/10.1016/j.cej.2023.147233

Oxygen Vacancy-enriched $V_2O_5 \cdot nH_2O$ Nanofibers Ink for Universal Substrates-tolerant and Multi Means-integratable NH_3 Sensing

Xiaxia Xing [a], Xinhua Zhao [a], Zhenxu Li [a], Lingling Du [a], Chen Wang [a], Dongliang Feng [a], Dongsheng Geng [b], Robert Bogdanowicz [c], Dachi Yang [a,*]

[a] Tianjin Key Laboratory of Optoelectronic Sensor and Sensing Network Technology, Engineering Research Center of Thin Film Optoelectronics Technology, Ministry of Education and Department of Electronics, College of Electronic Information and Optical Engineering, Nankai University, Tianjin 300350, P. R. China

E-mail: yangdachi@nankai.edu.cn

[b] School of Materials Science and Engineering, University of Science and Technology Beijing, Beijing, 100083, P. R. China

[c] Department of Metrology and Optoelectronics, Faculty of Electronics, Telecommunications and Informatics, Gdansk University of Technology, 11/12G. Narutowicza St., 80-233 Gdansk, Poland

Abstract：Universal substrates-tolerant and multi means-integratable ammonia (NH_3) sensing is highly desired in future Internet of Things in environmental monitoring, food security and early diagnosis of human diseases, however, is still less than satisfactory. Here, an oxygen vacancy-governed NH_3 sensing has been developed with $V_2O_5 \cdot nH_2O$ nanofibers (NFs) ink, via combined thermal decomposition of ammonium metavanadate and dilution. As-obtained NH_3 sensing ink takes on red colloids, in which the $V_2O_5 \cdot nH_2O$ NFs around 14 nm in diameter are interconnected. Beneficially, the fabric fiber decorated with $V_2O_5 \cdot nH_2O$ NFs ink displays excellent selectivity and ppb-concentration detection limit. Remarkably, $V_2O_5 \cdot nH_2O$ NFs ink is integrated over "hard" and "flexible" substrates such as glass, wood, paper, leaf and fabric with excellent tolerance by multi-integratable means such as writing, dipping and sewing. Theoretically, such NH_3 sensing is interpreted that the bonding between V_2O_5 NFs and H_2O modulates oxygen vacancy and thus adsorption sites, and the incorporation between crystal water and free one contributes to stable ink. Practically, A sensing device built with $V_2O_5 \cdot 3.1H_2O$ NFs ink has been simulated to communicate with a smartphone with reliable NH_3 sensing.

Keywords: Oxygen vacancy; $V_2O_5 \cdot nH_2O$ nanofibers sensing ink; Universal substrates-tolerant; Multi means-integratable; Ammonia sensing

1. Introduction

Ammonia (NH_3), as a promising energy carrier [1, 2], may damage human organs if the long-term exposure to NH_3 is larger than 25 ppm due to its corrosive and toxic nature [3, 4]. Instead, NH_3 may serve as a tracer of food spoilage [5] and an exhaled biomarker of impaired kidney [6] and liver function. As such, NH_3 sensing is potentially utilized in intelligent environmental monitoring, food security and early diagnosis of human diseases, which is simultaneously required with excellent selectivity and stability, and ppb-level detection limit. Generally, a universal substrates-tolerant and multi means-integratable NH_3 sensing may contribute to intelligent monitoring in the upcoming Internet of Things, although great progress has been made, it needs further exploring.

Actually, an NH_3 sensing material with modulated sensing performance plays a crucial role in the compatible integration over universal substrates by available means. As the NH_3 sensing materials, semiconducting metal oxides (SMOs) have been widely investigated [7-9], however, their challenging issues may limit their future applications. Firstly, oxygen vacancy may contribute to gas sensing of SMOs materials. Theoretically, the reaction between reducing gas such as NH_3 and ionized oxygen species would be boosted due to the enhanced adsorption of O_2 on oxygen vacancy [10, 11]. Accordingly, the means that can generate more oxygen vacancies such as H_2 plasma treatment [12], doping [13] and annealing [10, 11] have been utilized to improve the sensing performance, however, the strategies needs further developing. Secondly, the nano/micro-structured NH_3 sensing SMOs are usually endowed with powder form, and their suspension in an aqueous solution may agglomerate and peel off the utilized substrate [14, 15]. Even being temporarily integrated, further mechanical manipulation may also cause similar peeling off [16]. Thirdly, the tolerance of the sensing materials to universal substrates by facially integrating means is still less than satisfactory. Conductive polymers (CPs) as NH_3 sensing materials have been integrated over "hard" substrates such as glass [17] and ceramic [18] and "flexible" substrates such as polyethylene terephthalate (PET) [19] and paper [20]. Nevertheless, the substrates are still limited and their available integratable means require either complicated procedures or proficient technicians [6, 19]. Ideally, a NH_3 sensing material is tolerant to various substrates by multi-integratable means and its sensing performance can be improved by an ingenious strategy, however, little has been reported so far.

V_2O_5 as a transition metal oxide presents unique electrical and sensing performance [21], in which vanadium ions (V^{5+}) with an oxidation state generate the active sites for adsorbing gaseous molecules and catalyze reactions [22]. Compared with crystalline V_2O_5, $V_2O_5{\cdot}nH_2O$ has been investigated with a low crystallization, which is subjected to less mechanical stress and thus offers more active sites than their crystalline counterparts during reaction [23]. Notably, the presence of crystal water has been reported to boost the electrochemical reaction kinetics [24]. Being inspired, an oxygen vacancy-enriched $V_2O_5{\cdot}\ nH_2O$ nanofibers (NFs) ink with a sol form in this study has been developed for universal substrates-tolerant and multi means-integratable NH_3 sensing at room temperature. As characterized, the $V_2O_5{\cdot}nH_2O$ NFs of ~14 nm in diameter are interconnected to form red and highly dispersed ink with a zeta potential of ~ 38.8 mV. Beneficially, the response of diluted $V_2O_5{\cdot}3.1H_2O$ NFs fabric to 10 ppm NH_3 have been improved (S = 17.8%) compared with that of pristine one (S = 8.6%). Furthermore, the diluted $V_2O_5{\cdot}3.1H_2O$ NFs fabric fiber shows 100 ppb detection limit of NH_3 and excellent selectivity. Remarkably, the $V_2O_5{\cdot}nH_2O$ NFs ink has been integrated on various substrates such as ceramics, glass, wood, paper, fabric and leaf, by which multi-integratable means of writing, dipping and sewing have been applied. Such sensing ink would contribute to the diversification of NH_3 sensors in future intelligent sensing.

2. Experimental section

2.1 Synthesis of $V_2O_5 \cdot 2.3H_2O$ NFs ink [25]

Firstly, 1 g ammonium metavanadate (NH_4VO_3) was ground with deionized (D.I.) water, and then the fluid was mixed with 10 mL of 1M HCl under continuous stirring. Secondly, when the suspension turns red, D.I. water was added to make the total volume of 20 mL, the supernatant was removed after precipitation. Thirdly, the red precipitate was dispersed into 80-90 ºC hot water to a total volume of 20 mL, the supernatant was removed after stirring and precipitating. Finally, the dark red $V_2O_5 \cdot 2.3H_2O$ NFs dispersions were filled with 80-90 ºC hot water to a total volume of 40 mL for the subsequent utilization.

2.2 Synthesis of sensing fabrics and fabrics fiber integrating $V_2O_5 \cdot nH_2O$ NFs ink

Synthesis of $V_2O_5 \cdot nH_2O$ NFs fabrics is briefly described as follows. Initially, 0.5 mL, 2 mL and 5 mL of the above synthesized $V_2O_5 \cdot 2.3H_2O$ NFs ink were ultrasonically dispersed in 10 mL D.I. water, respectively. Correspondingly, they are denoted as ink-0.5, ink-2 and ink-5 in Fig. 3a, respectively. Secondly, the rectangular polyester fabric (2 cm×0.5 cm) and fabric fiber (Diameter: ~ 207 μm, Length: ~ 2 cm) was immersed in the above synthesized $V_2O_5 \cdot nH_2O$ NFs dispersion for 1 min. Finally, the $V_2O_5 \cdot nH_2O$ NFs fabrics and fabric fiber were dried at room temperature. In the same way, the sensing ink was integrated over the PET and paper in Fig. 5e. It should be noted that 2 mL of the pristine $V_2O_5 \cdot 2.3H_2O$ NFs ultrasonically dispersed in 10 mL D.I. water was defined as diluted $V_2O_5 \cdot 3.1H_2O$ NFs ink, which was taken as an example for deep investigation.

2.3 Synthesis of $V_2O_5 \cdot 2.3H_2O$ NFs aerogel and powder, and V_2O_5 NFs powder

The $V_2O_5 \cdot 2.3H_2O$ NFs ink was firstly frozen at -18 ℃ and then lyophilized at -51 ℃ in a freeze-drier (FD-1A-50, Henan Brothers Instrument and Equipment Co., Ltd., China) to obtain $V_2O_5 \cdot 2.3H_2O$ NFs aerogel. The $V_2O_5 \cdot 2.3H_2O$ NFs aerogel was grounded using an agate mortar to obtain $V_2O_5 \cdot 2.3H_2O$ NFs powder, its resistivity was tested under various pressures (2-30 MPa) in Fig. S1, in which the resistivity mean is ~ 7823 Ωcm. The $V_2O_5 \cdot 2.3H_2O$ NFs powder was annealed in air at 600 ºC for 2 h to remove the crystal water, then the V_2O_5 NFs powder was collected.

2.4 Characterization

The samples were characterized by field emission scanning electron microscopy (FE-SEM, JSM-7800) with energy dispersive X-ray spectroscopy (EDS, Oxford), transmission electron microscopy (TEM, JEM-2200FS), X-ray diffraction (XRD, Rigaku Smart Lab 3kW) using Cu Kα radiation, Raman spectra (SR-500I-A, a wavelength of 532 nm as the excitation), Ultraviolet-visible diffuse reflectance spectra (Shimadzu UV-3600), Mott-Schottky test (electrochemistry workstation VersaSTAT 4, AMETEK Princeton), thermogravimetric analysis (TGA) (Netzsch STA449F5 instrument, temperature range 30-600 ℃, heating rate 10 ℃/min, in nitrogen atmosphere), Automatic powder resistivity tester (ST2742B), Zeta potential analyzer (Malvern Zetasizer Nano ZS ZEN3600, UK), electron paramagnetic resonance (EPR) spectroscopy (Bruker EMXPLUS) and X-ray photoelectron spectroscopy (XPS, Thermo Scientific ESCALAB 250Xi). The XPS spectra on binding energies of various elements have been calibrated with C 1s at 284.8 eV.

2.5 Gas sensing measurement

The gas sensing was tested at room temperature (RT, ~ 25 °C) in air atmosphere. In detail, the two ends of fabric were connected to the Data Acquisition System (KEITHLEY 2701) by two gold clamps, which were placed in a homemade test chamber of 18 L with two air fans and a vaporizer. Notably, the NH_3 sensing is *in-situ* detection directly without other electrodes. Additionally, the gaseous and dry NH_3 with high-purity was adopted. The calculation of NH_3 concentration is conducted by the gas distribution formula (equation 1), in which C (ppm) and φ represent the target gas concentration and volume fraction, respectively, and V_1 (mL) and V_2 (mL) are denoted as the volume of target gas and testing chamber (V_2 = 18 L). The sensing response is expressed by $S = (R_g/R_a\text{-}1) *100\%$, of which R_a and R_g are the resistances in the air and target gas, respectively. The response/recovery time is defined as the time taken by the sensor to reach 90% of the final steady-state resistance after injecting or switching off the target gas.

$$V_1 = \frac{V_2 \times C}{\varphi} \times 10^{-6} \quad (1)$$

3. Results and Discussion

3.1. Synthesis and characterization

In Fig. 1a, the pristine $V_2O_5{\cdot}nH_2O$ NFs ink was diluted and integrated over fabrics, and the synthetic details of pristine $V_2O_5{\cdot}nH_2O$ NFs ink were provided in above experimental section. Meanwhile, the three-dimensional (3D) crystal structure of $V_2O_5{\cdot}nH_2O$ NFs was simulated by Visualization for Electronic and STructural Analysis (VESTA) [26]. Also, the X-ray diffractions (XRD) of pristine and diluted $V_2O_5{\cdot}nH_2O$ NFs were conducted (Fig. S2a) with the diffractive peak of $V_2O_5{\cdot}nH_2O$ at ~ 10° [27]. Meanwhile, the crystal water was removed by annealing the pristine $V_2O_5{\cdot}nH_2O$ NFs, and was then confirmed as the V_2O_5 (PDF#89-0612) in Fig. S2b. Further, Raman spectra of pristine $V_2O_5{\cdot}nH_2O$ NFs (Fig. S2c) show the V-O Raman scattering peaks with the orthorhombic crystalline [28]. Remarkably, the thermogravimetric analysis (TGA) was carried out to determine the "n" value in $V_2O_5{\cdot}nH_2O$ NFs. In Fig. 1b, weight loss of 23.4% and 18.6% occur at 100 - 600 °C, which is attributed to the loss of crystal water, and the "n" values corresponding to diluted and pristine $V_2O_5{\cdot}nH_2O$ NFs are 3.1 and 2.3, respectively. Specifically, the detailed calculation of "n" value in $V_2O_5{\cdot}nH_2O$ is described as follows. M, m_p and m_d represent relative molecular mass, mass of pristine $V_2O_5{\cdot}nH_2O$ NFs and mass of diluted one, respectively. Therefore, the "n" values corresponding to the diluted and pristine ones are calculated by the bellow proportional formula of the chemical equation.

	$V_2O_5{\cdot}nH_2O$	→	V_2O_5
M:	181.88 + n*18		181.88
m_p:	4.198 g		4.198 g*(1-18.6%)
m_d:	3.933 g		3.933 g*(1-23.4%)

In Fig. 1c, $V_2O_5{\cdot}3.1H_2O$ NFs ink is observed dense and overlapped in a lower magnification with scanning electron microscopy (SEM). While in a closer observation under transmission electron microscopy (TEM), the diameter of $V_2O_5{\cdot}nH_2O$ NFs in Fig. 1d is measured ~ 14 nm (Fig. S3). Moreover, the high-resolution TEM (HR-TEM) image and selected area electron diffraction (SAED) pattern in Fig. 1f and Fig. S4 show the (102) plane of

V_2O_5 (PDF#89-0612). Further, the elemental mappings under TEM (Fig. S5) verified the existence of V and O elements, and the diameter of the fabric fiber integrated with diluted $V_2O_5 \cdot 3.1H_2O$ NFs ink was measured ~ 207 μm in Fig. $1g_1$. By comparing with the shape of pristine fabric fiber in Fig. $1h_1$, the flake shape in Fig. $1g_2$ reveals that the $V_2O_5 \cdot 3.1H_2O$ NFs ink has been integrated over fabrics. Interestingly, the Tyndall effects of pristine and various diluted ink were compared in Fig. S6, the dispersibility of pristine $V_2O_5 \cdot 2.3H_2O$ NFs ink can be improved via dilution.

3.2. The stable $V_2O_5 \cdot nH_2O$ NFs ink for dilution-modulated NH_3 sensing

To get insight into the role of water in $V_2O_5 \cdot nH_2O$ NFs ink, the free water was initially removed by freezing and drying $V_2O_5 \cdot 2.3H_2O$ NFs ink, and then the lyophilized ones were annealed to remove crystal water and obtain V_2O_5 for subsequent comparison. In Fig. S7, the color of $V_2O_5 \cdot 2.3H_2O$ NFs powder changed from its pristine dark red to orange after annealing. The V_2O_5 and $V_2O_5 \cdot 2.3H_2O$ NFs powder were ultrasonically dispersed into D.I. water and pure ethanol, respectively. Correspondingly, various dispersions were dripped over interdigital electrodes in Fig. 2d for comparing their NH_3 sensing performance, and the real-time resistance curves were shown in Fig. 2a.

In Fig. 2b-c, the $V_2O_5 \cdot 2.3H_2O$ NFs exhibit a higher response to 10 ppm NH_3 than that of V_2O_5 NFs in both water and pure ethanol solvent, revealing the crystal water-boosted NH_3 sensing. Actually, water solvent may contribute to lower baseline resistance in both V_2O_5 and $V_2O_5 \cdot nH_2O$ NFs (Fig. 2c). Further, free water is required in preparing $V_2O_5 \cdot nH_2O$ NFs ink in Fig. 2e. Otherwise, uneven and unstable dispersion can be obtained. Meanwhile, the $V_2O_5 \cdot 2.3H_2O$ NFs ink and ethanol dispersion were dipped over fabric in Fig. $2d_1$. In Fig. S8, the resistance value of $V_2O_5 \cdot 2.3H_2O$ NFs ink fabric is ~ 0.49 MΩ, however, the one with ethanol dispersion is larger than 20 MΩ, which reveals that the uniform and stable $V_2O_5 \cdot 2.3H_2O$ NFs ink contribute to integrating conductive fabric. Notably, if one deliberately removed the crystal water in $V_2O_5 \cdot 2.3H_2O$ NFs or replaced the dispersion medium from water to pure ethanol, the dispersed phase is obviously separated from dispersion medium (Fig. 2e), rather than obtaining stable ink. As such, the incorporation of crystal water bonded by V_2O_5 with free water in the dispersion medium plays a pivotal role in the formation of sensing ink.

The diluted $V_2O_5 \cdot 3.1H_2O$ and pristine $V_2O_5 \cdot 2.3H_2O$ NFs inks were observed with the variation of Tyndall effect in Fig. 2f and g, in which the light path penetrates after diluting with high dispersibility of colloid [29]. Meanwhile, the simulated 3D crystalline structures with various oxygen vacancies of diluted and pristine $V_2O_5 \cdot nH_2O$ NFs are shown in Fig. $2f_1$ and g_1, respectively. With the pristine $V_2O_5 \cdot 2.3H_2O$ NFs ink for comparisons, the diluted $V_2O_5 \cdot 3.1H_2O$ NFs ink was integrated over the fabric (2 cm×0.5 cm) and the fabric fiber (Diameter: ~ 207 μm, Length: ~ 2 cm), respectively. In the photographs of Fig. 2f and g, the color of diluted $V_2O_5 \cdot 3.1H_2O$ NFs fabrics was seen lighter than that of pristine $V_2O_5 \cdot 2.3H_2O$ ones. To further gain insight into the role of dilution, the NH_3 sensing performance of the above integrated various pristine $V_2O_5 \cdot 2.3H_2O$ and diluted $V_2O_5 \cdot 3.1H_2O$ NFs fabric were investigated with comparison. In Fig. 2h, the recovery speed of pristine $V_2O_5 \cdot 2.3H_2O$ NFs fabric is improved by both diluting and adopting the fabric fiber. Meanwhile, the responses toward 5 ppm and 25 ppm NH_3 were summarized in Fig. 2i, and show that the sensing responses of diluted $V_2O_5 \cdot 3.1H_2O$ NFs ink onto both fabric and fabric fiber are higher than those of pristine ones. Moreover, the real-time responses to 1-50 ppm NH_3 were evaluated in Fig. 2j, which further reveals the dilution improved NH_3 sensing performance.

3.3. Evaluation of the NH_3 sensing performance

The content of $V_2O_5 \cdot nH_2O$ NFs in the sensing ink governs the NH_3 sensing. In Fig. 3a, the responses of pristine and various diluted $V_2O_5 \cdot nH_2O$ NFs fabric to 10 ppm NH_3 were evaluated, and the $V_2O_5 \cdot nH_2O$-2 mL NFs fabric manifested the highest response (S = 17.8%) compared with pristine ones (S = 8.6%), and was thus chosen for subsequent evaluation and renamed by $V_2O_5 \cdot 3.1H_2O$ NFs fabric. The response and recovery time were evaluated to ~ 75 s and 36 s toward 1 ppm NH_3 in Fig. S9, respectively. Remarkably, the flexibility of $V_2O_5 \cdot nH_2O$ NFs fabric was investigated by testing their responses to 1 ppm and 10 ppm NH_3 upon the bending angle at 0^o, 45^o, 90^o and 360^o, respectively. Excitedly, little difference was observed in Fig. 3b, indicating excellent flexibility.

The stability and selectivity are crucial parameters for NH_3 sensing. Remarkably, the sensing evaluation to 5 ppm NH_3 is repeated for 126 days' durations in Fig. 3c with good stability. Furthermore, the responses of various interfering gases and 10 ppm target NH_3 were compared in Fig. 3d, revealing excellent selectivity. Meanwhile, the NH_3 sensing of three $V_2O_5 \cdot 2.3H_2O$ NFs fabrics in Fig. S10 is compared, which shows a slight variation in response to the same concentration NH_3 and takes a good consistency. Additionally, the diluted $V_2O_5 \cdot 3.1H_2O$ NFs ink was integrated over the fabric fiber in Fig. 3e, and its low detection limit is around 100 ppb NH_3. Towards a low NH_3 concentration (e.g., 100 ppb-1 ppm), the responses show an excellent linear relationship in Fig. 3f. While towards a high one (e.g., 1-50 ppm), excellent repeatability is observed in Fig. 3g. As a result, the $V_2O_5 \cdot nH_2O$ NFs fabric simultaneously present ppb-level detection, high selectivity and stability, excellent flexibility and low working temperature. Compared with other SMOs NH_3 sensing materials in Table 1, a gel-stated and stable ink of $V_2O_5 \cdot nH_2O$ NFs is prepared, which can be integrated over various "hard" and "flexible" substrates by multi-integratable means.

In our experiments, both temperature and humidity can influence the NH_3 sensing. In Fig. S11, the temperature-dependent sensing responses were observed to 20 ppm NH_3 at ~ 26-140 ^oC, and the highest one takes place at room temperature (~ 26 ^oC). Meanwhile, the baseline resistance and the sensing response of $V_2O_5 \cdot 3.1H_2O$ NFs fabric toward 5 ppm NH_3 decrease with humidity (Fig. S12), similar to previous SMOs [30] and to other humidity sensors [31]. Such a decrease in the sensing response might be interpreted that H_2O molecules occupy adsorption sites, which weakens the reaction between NH_3 and adsorbed oxygen onto the surface of $V_2O_5 \cdot 3.1H_2O$ NFs [32], as may be addressed by covering filter membrane [33].

3.4. The oxygen vacancy governed NH_3 sensing mechanism

We experimentally investigated the chemisorbed oxygen to understand the dilution-boosted NH_3 sensing mechanism, and three characterizations on oxygen vacancy ($V_o^{\cdot}$) of diluted $V_2O_5 \cdot 3.1H_2O$ NFs were performed with pristine $V_2O_5 \cdot 2.3H_2O$ ones as comparison. Firstly, the O 1s X-ray photoelectron spectroscopy (XPS) in Fig. 4a spectra were deconvoluted into three oxygen species of O_I, O_{II} and O_{III}, which are associated with oxygen atoms bound to metals, defect sites with low oxygen coordination and hydroxy species, respectively. Remarkably, the integral-area ratios of O_{II} increase from 20% of pristine $V_2O_5 \cdot 2.3H_2O$ NFs to 52% of diluted $V_2O_5 \cdot 3.1H_2O$ ones, indicating that the diluted $V_2O_5 \cdot 3.1H_2O$ one possesses more oxygen vacancies [34]. Meanwhile, the V 2p spectra in Fig. 4b correspond to the characteristics of V^{5+}, the discrepancy in binding energy (0.3 eV) indicates distinct electronic environments of V ions in the pristine and diluted $V_2O_5 \cdot nH_2O$ NFs, which might be interpreted as increased oxygen vacancy in the diluted $V_2O_5 \cdot 3.1H_2O$ ones [10]. Secondly, the presence of oxygen vacancy was further studied by electron paramagnetic resonance (EPR) spectroscopic measurements in Fig. 4c and symmetrical EPR signals (g = 1.9612) are assigned to the unpaired electrons in the oxygen vacancy sites [10, 35]. The ESR intensity of diluted $V_2O_5 \cdot 3.1H_2O$ NFs is higher than

that of pristine $V_2O_5 \cdot 2.3H_2O$ ones, indicating dilution governed the oxygen vacancy, which result in more chemisorbed oxygen for gas sensing. Thirdly, such result is also evidenced by the narrower optical bandgaps (E_g) of diluted $V_2O_5 \cdot 3.1H_2O$ NFs (1.87 eV) than that of pristine $V_2O_5 \cdot 2.3H_2O$ (2.19 eV) in Fig. 4d.

The energy-band variation of $V_2O_5 \cdot nH_2O$ NFs was investigated for understanding the NH_3 sensing mechanism. Specifically, the valence band maximum (E_v) of the $V_2O_5 \cdot 3.1H_2O$ NFs is determined to ~ 2.4 eV (Fig. S14). Accordingly, the conduction band minimum (E_c) of $V_2O_5 \cdot 3.1H_2O$ is calculated to ~ 0.53 eV according to Equation (2). Usually, V_2O_5 is reported as a n-type semiconductor [36]. However, p-type sensing characteristic with increased resistance was observed in this study (Fig. 2a and h) , which is explained as follows. The $V_2O_5 \cdot 3.1H_2O$ NFs contain abundant oxygen vacancy, which will improve chemisorption of O_2 and H_2O molecule [11, 37], capture more electrons from the conduction band of $V_2O_5 \cdot nH_2O$ NFs and thus bend upward band causing an inversion layer, therefore, the Fermi level (E_F) located below the intrinsic level (E_i) in Fig. 4e [38]. In the surface inversion layer, holes usually serve as the major carriers with p-type feature, which was confirmed by Mott-Schottky with a negative slope in Fig. $4e_1$.

$$E_c = E_v - E_g \quad (2)$$

To understand the p-type sensing mechanism, the NH_3 sensing evaluations under various working temperatures were investigated in Fig. S11, the $V_2O_5 \cdot 3.1H_2O$ NFs show increased sensing resistance to 20 ppm NH_3 at ~ 26-80 ^oC and decreased ones at ~ 100-140 ^oC. Such phenomenon is explained as follows. At lower temperatures, the strong adsorption of O_2 and H_2O molecules contribute to the formation of an inversion layer on the surface of $V_2O_5 \cdot 3.1H_2O$ NFs, exhibiting p-type semiconductor properties [39]. With the elevating of temperature, an inversion layer would be destroyed without sufficient O_2 and H_2O molecules, n-type sensing behavior would be seen. Further, we conducted additional comparative experiments on NH_3 sensing under insufficient oxygen conditions and air atmosphere in Fig. S15, the significantly decreased response in Fig. S15a indicates that the sufficient surface adsorption of oxygen contributes to NH_3 sensing of $V_2O_5 \cdot 3.1H_2O$ NFs.

Accordingly, the NH_3 sensing mechanism of $V_2O_5 \cdot nH_2O$ NFs fabrics is interpreted as follows. In Fig. 4f, when the pristine p-type $V_2O_5 \cdot 2.3H_2O$ ones are exposed to NH_3, the pre-adsorbed oxygen species (O_2^-) and hydroxy species (-OH) react with NH_3 and release electrons [40, 41], reducing the hole concentration and thus elevating the resistance. Similarly, the diluted $V_2O_5 \cdot 3.1H_2O$ NFs show NH_3 sensing mechanism in Fig. $4f_1$. However, the content of their oxygen vacancy is significantly increased thus improved chemisorbed oxygen, and finally present boosted NH_3 sensing.

3.5. $V_2O_5 \cdot nH_2O$ NFs ink for universal substrates-tolerant and multi means-integratable NH_3 sensing and the simulation detection of NH_3

The universal-substrates tolerance and multi-means integration of $V_2O_5 \cdot 2.3H_2O$ NFs ink were investigated. The tolerance has been widely examined on hard substrates such as ceramics, stainless steel, glass and wood, and flexible ones such as Chinese “Xuan” paper, leaf, Al foil, plastic wrap and A4 size paper in Fig. 5a. Meanwhile, the adhesive performance of the $V_2O_5 \cdot 2.3H_2O$ NFs ink over the above substrate has been investigated in Fig. S16, one can see that the adhesive properties depend on the substrates and the sensing ink shows a weaker adhesion than that of commercial one on A4 paper (Fig. S17). As for the integratable means, our $V_2O_5 \cdot 2.3H_2O$ NFs ink can be dipped with a paintbrush to draw the school badge and the motto of Nankai University in Fig. 5a and other “dipping-drying” approach in Fig. 5b.

Impressively, the $V_2O_5 \cdot 3.1H_2O$ NFs ink can also serve as a colouring agent with color variation from white of pristine fabric fiber to orange, which can be integrated over the fabric fiber (Fig. 5c), and can even be sewed on the clothes with the "NKU" pattern. Particularly, by freezing and drying, the $V_2O_5 \cdot 3.1H_2O$ NFs ink can be transformed into lightweight aerogel, and can even stand on the tip of the reed (Fig. S18). In this case, even being storing 365 days (Fig. 5d) and 608 days (Fig. S19a), the $V_2O_5 \cdot 3.1H_2O$ NFs ink remains excellent dispersibility and stability, which is verified by characterizing the zeta potential of $V_2O_5 \cdot 3.1H_2O$ NFs ink to ~ 38.8 mV after storing 608 days (Fig. S19b).

As examples, the PET, Chinese "Xuan" paper and fabric integrated with $V_2O_5 \cdot 3.1H_2O$ NFs ink were examined for their NH_3 sensing performance in Fig. 5e, showing substrates-dependent NH_3 sensing, which may be explained that these bare and insulated substrates serve as support and don't participate electron transport. Although previous investigations (Table 1) have made great progress, our $V_2O_5 \cdot nH_2O$ NFs ink is the one that can be simultaneously utilized for universal substrates-tolerant and multi means-integratable NH_3 sensing. Practically, such NH_3 sensing ink enable to be integrated into the feasible substrates such as smocks, mask and food packaging bag for environmental monitoring, exhaled diagnosis of human diseases and inspection of food safety. Herein, we elaborately integrated the $V_2O_5 \cdot 3.1H_2O$ NFs ink onto the polyethylene sample bag (4 cm×6 cm) as an example, to simulate detection of NH_3, which was read by a smartphone (Fig. 5f). Specifically, the microcontroller NodeMCU (ESP8266, 5.8 cm×3.1 cm) with Wireless Fidelity (Wi-Fi) module communicate with the smartphone and perform the NH_3 sensing and alarming of the device. In the supplemental video, when 10 ppm NH_3 was injected and the sensing voltage is lower than the alarm threshold (0.5 V), the smartphone read "AlARMING!" (Fig. 5g). Conversely, the NH_3 being released with the one higher than 0.5 V, and "Monitoring" in smartphone is seen. Also, the detailed historical information can be read and recorded in Fig. 5h, which is great potential for inspection of food safety.

4. Conclusion

To summarize, an oxygen vacancy-enriched $V_2O_5 \cdot nH_2O$ NFs ink has been developed by combining the thermal decomposition of ammonium metavanadate with subsequent dilution, for universal substrates-tolerant and multi means-integratable NH_3 sensing at room temperature. Experimentally, the $V_2O_5 \cdot nH_2O$ NFs of ~ 14 nm in diameter were observed to be interconnected, forming red colloids in an aqueous solution with high dispersibility. Theoretically, the bonding between V_2O_5 NFs and H_2O governs the oxygen vacancy with improved the adsorption sites of NH_3, and the incorporation between crystal water and free water contributes to stable ink. Beneficially, the diluted $V_2O_5 \cdot 3.1H_2O$ NFs fabrics show an increased response to 10 ppm NH_3 (S = 17.8%) compared with the pristine ones (S = 8.6%). Also, the $V_2O_5 \cdot nH_2O$ NFs ink fabric fiber displays excellent selectivity and ppb-level detection limit to NH_3. Remarkably, $V_2O_5 \cdot nH_2O$ NFs ink has been integrated over various substrates such as ceramics, glass, wood, paper, fabric and leaf with universal substrates-tolerance. Meanwhile, multiple strategies of writing, dipping and sewing have been adopted for integration. As an example of application, the developed oxygen vacancy-enriched $V_2O_5 \cdot 3.1H_2O$ NFs ink has been integrated into a sensing device and communicates with a smartphone with reliable monitoring and alarming, which is potential in future intelligent sensing of Internet of Things. Future investigations are expected to be conducted on theoretical calculations and humidity-dependent NH_3 sensing.

Declaration of Competing Interest

The authors declare that they have no known competing financial interests or personal relationships that could have appeared to influence the work reported in this paper.

Data availability

Data will be made available on request.

Acknowledgements

This work was financially supported by the National Natural Science Foundation of China (Grant No. 52072184) and Tianjin Research Innovation Project for Postgraduate Students (General Project, Grant No. 2022BKY035).

References

[1] W. Gao, J. Guo, P. Wang, Q. Wang, F. Chang, Q. Pei, W. Zhang, L. Liu, P. Chen, Production of ammonia via a chemical looping process based on metal imides as nitrogen carriers, Nat. Energy 3 (2018) 1067-1075.

[2] K. Nakajima, H. Toda, K. Sakata, Y. Nishibayashi, Ruthenium-catalysed oxidative conversion of ammonia into dinitrogen, Nat. Chem. 11 (2019) 702-709.

[3] M. Van Damme, L. Clarisse, S. Whitburn, J. Hadji-Lazaro, D. Hurtmans, C. Clerbaux, P.-F. Coheur, Industrial and agricultural ammonia point sources exposed, Nature 564 (2018) 99-103.

[4] A.T. Güntner, M. Wied, N.J. Pineau, S.E. Pratsinis, Rapid and Selective NH_3 Sensing by Porous CuBr, Adv. Sci. 7 (2020) 1903390.

[5] Z. Ma, P. Chen, W. Cheng, K. Yan, L. Pan, Y. Shi, G. Yu, Highly Sensitive, Printable Nanostructured Conductive Polymer Wireless Sensor for Food Spoilage Detection, Nano Lett. 18 (2018) 4570-4575.

[6] H.-Y. Li, C.-S. Lee, D.H. Kim, J.-H. Lee, Flexible Room-Temperature NH_3 Sensor for Ultrasensitive, Selective, and Humidity-Independent Gas Detection, ACS Appl. Mater. Interfaces 10 (2018) 27858-27867.

[7] B. Yang, X. Li, W. Yuan, Z. Li, N. Lu, S. Wang, Y. Wu, S. Fan, Z. Hua, Efficient NH_3 Detection Based on MOS Sensors Coupled with Catalytic Conversion, ACS Sens. 5 (2020) 1838-1848.

[8] S. Kumar, A. Singh, R. Singh, S. Singh, P. Kumar, R. Kumar, Facile h-MoO_3 synthesis for NH_3 gas sensing application at moderate operating temperature, Sens. Actuator B Chem. 325 (2020) 128974.

[9] Y.-Y. Li, J.-L. Chen, F.-L. Gong, G.-X. Jin, K.-F. Xie, X.-Y. Yang, Y.-H. Zhang, Dual functionalized Ni substitution in shuttle-like In_2O_3 enabling high sensitivity NH_3 detection, Appl. Surf. Sci. 600 (2022) 154158.

[10] H. Yuan, S.A.A.A. Aljneibi, J. Yuan, Y. Wang, H. Liu, J. Fang, C. Tang, X. Yan, H. Cai, Y. Gu, S.J. Pennycook, J. Tao, D. Zhao, ZnO Nanosheets Abundant in Oxygen Vacancies Derived from Metal-Organic Frameworks for ppb-Level Gas Sensing, Adv. Mater. 31 (2019) 1807161.

[11] G. Li, H. Zhang, L. Meng, Z. Sun, Z. Chen, X. Huang, Y. Qin, Adjustment of oxygen vacancy states in ZnO and its application in ppb-level NO_2 gas sensor, Sci. Bull. 65 (2020) 1650-1658.

[12] Z. Geng, X. Kong, W. Chen, H. Su, Y. Liu, F. Cai, G. Wang, J. Zeng, Oxygen Vacancies in ZnO Nanosheets Enhance CO_2 Electrochemical Reduction to CO, Angew. Chem. Int. Ed. 57 (2018) 6054-6059.

[13] X. Wang, T. Wang, G. Si, Y. Li, S. Zhang, X. Deng, X. Xu, Oxygen vacancy defects engineering on Ce-doped α-Fe_2O_3 gas sensor for reducing gases, Sens. Actuator B Chem. 302 (2020) 127165.

[14] J.H. Kim, J.H. Han, Y.C. Jung, Y.A. Kim, Mussel adhesive protein-coated titanium oxide nanoparticles for effective NO removal from versatile substrates, Chem. Eng. J. 378 (2019) 122164.

[15] M.S. Azmina, R. Md Nor, H.A. Rafaie, N.S.A. Razak, S.F.A. Sani, Z. Osman, Enhanced photocatalytic activity of ZnO nanoparticles grown on porous silica microparticles, Appl. Nanosci. 7 (2017) 885-892.

[16] H.-R. Lim, H.S. Kim, R. Qazi, Y.-T. Kwon, J.-W. Jeong, W.-H. Yeo, Advanced Soft Materials, Sensor Integrations, and Applications of Wearable Flexible Hybrid Electronics in Healthcare, Energy, and Environment, Adv. Mater. 32 (2020) 1901924.

[17] C.-T. Lee, Y.-S. Wang, High-performance room temperature NH_3 gas sensors based on polyaniline-reduced graphene oxide nanocomposite sensitive membrane, J. Alloys. Compd. 789 (2019) 693-696.

[18] C. Liu, H. Tai, P. Zhang, Z. Ye, Y. Su, Y. Jiang, Enhanced ammonia-sensing properties of PANI-TiO_2-Au ternary self-assembly nanocomposite thin film at room temperature, Sens. Actuator B Chem. 246 (2017) 85-95.

[19] N. Tang, C. Zhou, L. Xu, Y. Jiang, H. Qu, X. Duan, A Fully Integrated Wireless Flexible Ammonia Sensor Fabricated by Soft Nano-Lithography, ACS Sens. 4 (2019) 726-732.

[20] L. Du, D. Feng, X. Xing, C. Wang, Y. Gao, S. Sun, G. Meng, D. Yang, Nanocomposite-Decorated Filter Paper as a Twistable and Water-Tolerant Sensor for Selective Detection of 5 ppb–60 v/v% Ammonia, ACS Sens. 7 (2022) 874-883.

[21] X. Sun, R. Gao, Y. Wu, X. Zhang, X. Cheng, S. Gao, Y. Xu, L. Huo, Novel in-situ deposited V_2O_5 nanorods array film sensor with enhanced gas sensing performance to n-butylamine, Chem. Eng. J. 459 (2023) 141505.

[22] N. Panahi, M. Shirazi, M.T. Hosseinnejad, Fabrication, characterization and hydrogen

gas sensing performance of nanostructured V_2O_5 thin films prepared by plasma focus method, J. Mater. Sci. Mater. El. 29 (2018) 13345-13353.

[23] A. Moretti, S. Passerini, Bilayered Nanostructured $V_2O_5{\cdot}nH_2O$ for Metal Batteries, Adv. Energy Mater. 6 (2016) 1600868.

[24] Q. Sun, H. Cheng, Y. Yuan, Y. Liu, W. Nie, K. Zhao, K. Wang, W. Yao, X. Lu, J. Lu, Uncovering the Fundamental Role of Interlayer Water in Charge Storage for Bilayered $V_2O_5 \cdot nH_2O$ Xerogel Cathode Materials, Adv. Energy Mater. 13 (2023) 2202515.

[25] K. Zhou, Y. He, Q. Xu, Q.e. Zhang, A.a. Zhou, Z. Lu, L.-K. Yang, Y. Jiang, D. Ge, X.Y. Liu, H. Bai, A Hydrogel of Ultrathin Pure Polyaniline Nanofibers: Oxidant-Templating Preparation and Supercapacitor Application, ACS Nano 12 (2018) 5888-5894.

[26] K. Momma, F. Izumi, VESTA3 for three-dimensional visualization of crystal, volumetric and morphology data, J. Appl. Cryst. 44 (2011) 1272-1276.

[27] C. Xiong, A.E. Aliev, B. Gnade, K.J. Balkus, Fabrication of Silver Vanadium Oxide and V_2O_5 Nanowires for Electrochromics, ACS Nano 2 (2008) 293-301.

[28] H. Zhang, X. Han, R. Gan, Z. Guo, Y. Ni, L. Zhang, A facile biotemplate-assisted synthesis of mesoporous V_2O_5 microtubules for high performance asymmetric supercapacitors, Appl. Surf. Sci. 511 (2020) 145527.

[29] Z. Zhao, X. Wang, X. Jing, Y. Zhao, K. Lan, W. Zhang, L. Duan, D. Guo, C. Wang, L. Peng, X. Zhang, Z. An, W. Li, Z. Nie, C. Fan, D. Zhao, General Synthesis of Ultrafine Monodispersed Hybrid Nanoparticles from Highly Stable Monomicelles, Adv. Mater. 33 (2021) 2100820.

[30] F. Qu, S. Zhang, C. Huang, X. Guo, Y. Zhu, T. Thomas, H. Guo, J.P. Attfield, M. Yang, Surface Functionalized Sensors for Humidity-Independent Gas Detection, Angew. Chem. Int. Ed. 60 (2021) 6561-6566.

[31] P. Guo, B. Tian, J. Liang, X. Yang, G. Tang, Q. Li, Q. Liu, K. Zheng, X. Chen, W. Wu, An All-Printed, Fast-Response Flexible Humidity Sensor Based on Hexagonal-WO_3 Nanowires for Multifunctional Applications, Adv. Mater. (2023) 2304420.

[32] K. Suematsu, M. Sasaki, N. Ma, M. Yuasa, K. Shimanoe, Antimony-Doped Tin Dioxide Gas Sensors Exhibiting High Stability in the Sensitivity to Humidity Changes, ACS Sens. 1 (2016) 913-920.

[33] D. Feng, L. Du, X. Xing, C. Wang, J. Chen, Z. Zhu, Y. Tian, D. Yang, Highly Sensitive and Selective NiO/WO_3 Composite Nanoparticles in Detecting H_2S Biomarker of Halitosis, ACS Sens. 6 (2021) 733-741.

[34] B. Zhang, L. Wang, Y. Zhang, Y. Ding, Y. Bi, Ultrathin FeOOH Nanolayers with Abundant Oxygen Vacancies on $BiVO_4$ Photoanodes for Efficient Water Oxidation, Angew. Chem. Int. Ed. 57 (2018) 2248-2252.

[35] B. Tong, Z. Deng, B. Xu, G. Meng, J. Shao, H. Liu, T. Dai, X. Shan, W. Dong, S. Wang, S. Zhou, R. Tao, X. Fang, Oxygen Vacancy Defects Boosted High Performance p-Type Delafossite $CuCrO_2$ Gas Sensors, ACS Appl. Mater. Interfaces 10 (2018) 34727-34734.

[36] K. Schneider, M. Lubecka, A. Czapla, V_2O_5 thin films for gas sensor applications, Sens. Actuator B Chem. 236 (2016) 970-977.

[37] D. Yao, C. Dong, Q. Bing, Y. Liu, F. Qu, M. Yang, B. Liu, B. Yang, H. Zhang, Oxygen-Defective Ultrathin $BiVO_4$ Nanosheets for Enhanced Gas Sensing, ACS Appl. Mater. Interfaces 11 (2019) 23495-23502.

[38] X. Xing, L. Du, D. Feng, C. Wang, M. Yao, X. Huang, S. Zhang, D. Yang, Individual gas sensor detecting dual exhaled biomarkers via a temperature modulated n/p semiconducting transition, J. Mater. Chem. A 8 (2020) 26004-26012.

[39] L. Xu, C. Wang, X. Zhang, D. Guo, Q. Pan, G. Zhang, S. Wang, NOx sensitivity of conductometric $In(OH)_3$ sensors operated at room temperature and transition from p- to n- type conduction, Sens. Actuator B Chem. 245 (2017) 533-540.

[40] H. Wu, J. Yu, G. Yao, Z. Li, W. Zou, X. Li, H. Zhu, Z. Huang, Z. Tang, Room temperature NH_3 sensing properties and humidity influence of $Ti_3C_2T_x$ and Ag-$Ti_3C_2T_x$ in an oxygen-free environment, Sens. Actuator B Chem. 369 (2022) 132195.

[41] D. Wang, D. Zhang, Y. Yang, Q. Mi, J. Zhang, L. Yu, Multifunctional Latex/Polytetrafluoroethylene-Based Triboelectric Nanogenerator for Self-Powered Organ-like MXene/Metal–Organic Framework-Derived CuO Nanohybrid Ammonia Sensor, ACS Nano 15 (2021) 2911-2919.

[42] Y. Liu, H. Ji, Z. Yuan, H. Zhu, L. Kong, H. Gao, F. Meng, Hollow urchin Co-Fe_2O_3 with outstanding selectivity and fast responding for ppb level NH_3 sensing via Lewis acid-base effect, Chem. Eng. J. 474 (2023) 145620.

[43] K.-P. Yuan, L.-Y. Zhu, J.-H. Yang, C.-Z. Hang, J.-J. Tao, H.-P. Ma, A.-Q. Jiang, D.W. Zhang, H.-L. Lu, Precise preparation of WO_3@SnO_2 core shell nanosheets for efficient NH_3 gas sensing, J. Colloid Interf. Sci. 568 (2020) 81-88.

[44] F. Ranjbar, S. Hajati, M. Ghaedi, K. Dashtian, H. Naderi, J. Toth, Highly selective MXene/V_2O_5/$CuWO_4$-based ultra-sensitive room temperature ammonia sensor, J. Hazard. Mater. 416 (2021) 126196.

[45] D. Maity, R.T.R. Kumar, Polyaniline Anchored MWCNTs on Fabric for High Performance Wearable Ammonia Sensor, ACS Sens. 3 (2018) 1822-1830.

[46] D. Lv, W. Shen, W. Chen, R. Tan, L. Xu, W. Song, PSS-PANI/PVDF composite based flexible NH_3 sensors with sub-ppm detection at room temperature, Sens. Actuator B Chem. 328 (2021) 129085.

[47] D. Zhang, Y. Yang, Z. Xu, D. Wang, C. Du, An eco-friendly gelatin based triboelectric nanogenerator for a self-powered PANI nanorod/$NiCo_2O_4$ nanosphere ammonia gas sensor, J. Mater. Chem. A 10 (2022) 10935-10949.

[48] X. Wang, D. Zhang, H. Zhang, L. Gong, Y. Yang, W. Zhao, S. Yu, Y. Yin, D. Sun, In situ polymerized polyaniline/MXene (V_2C) as building blocks of supercapacitor and ammonia sensor self-powered by electromagnetic-triboelectric hybrid generator, Nano Energy 88 (2021) 106242.

[49] Y. Fu, T. Wang, X. Wang, X. Li, Y. Zhao, F. Li, G. Zhao, X. Xu, Investigation of p-n

505 sensing transition and related highly sensitive NH_3 gas sensing behavior of SnPx/rGO
506 composites, Chem. Eng. J. 471 (2023) 144499.

507

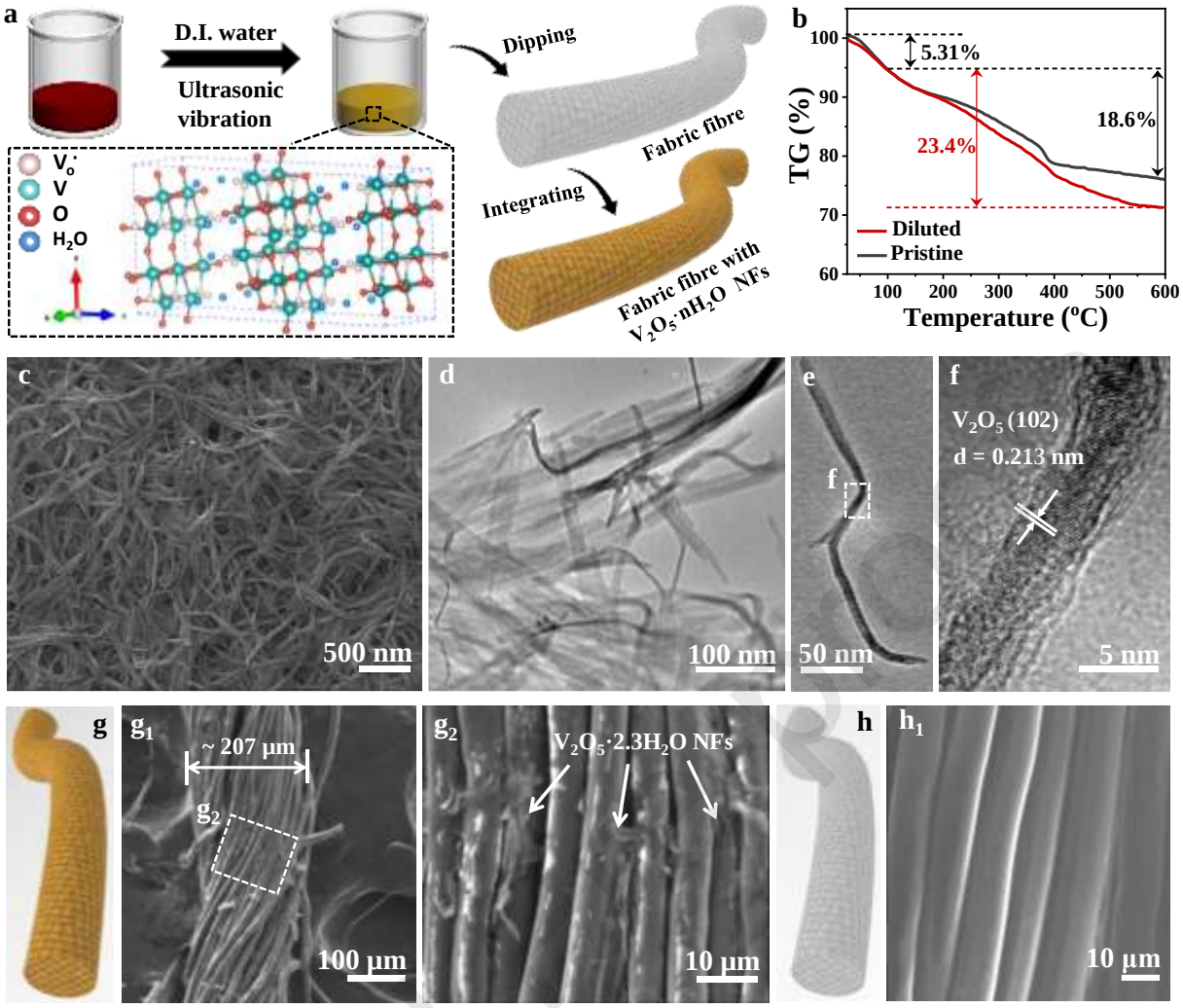

Fig. 1. The synthesis and characterization of $V_2O_5{\cdot}nH_2O$ NFs. (a) The schematic diagram of diluting and integrating $V_2O_5{\cdot}nH_2O$ NFs ink, and the simulated crystal structure of $V_2O_5{\cdot}nH_2O$ NFs. (b) The TGA curves of pristine and diluted $V_2O_5{\cdot}nH_2O$ NFs. (c) The SEM, (d-e) TEM and (f) HRTEM images of pristine $V_2O_5{\cdot}2.3H_2O$ NFs. (g) The schematic diagram and (g_1-g_2) SEM images of fabric fiber integrated with $V_2O_5{\cdot}nH_2O$ NFs ink. (h) The schematic diagram and (h_1) the SEM image of bare fabric fiber.

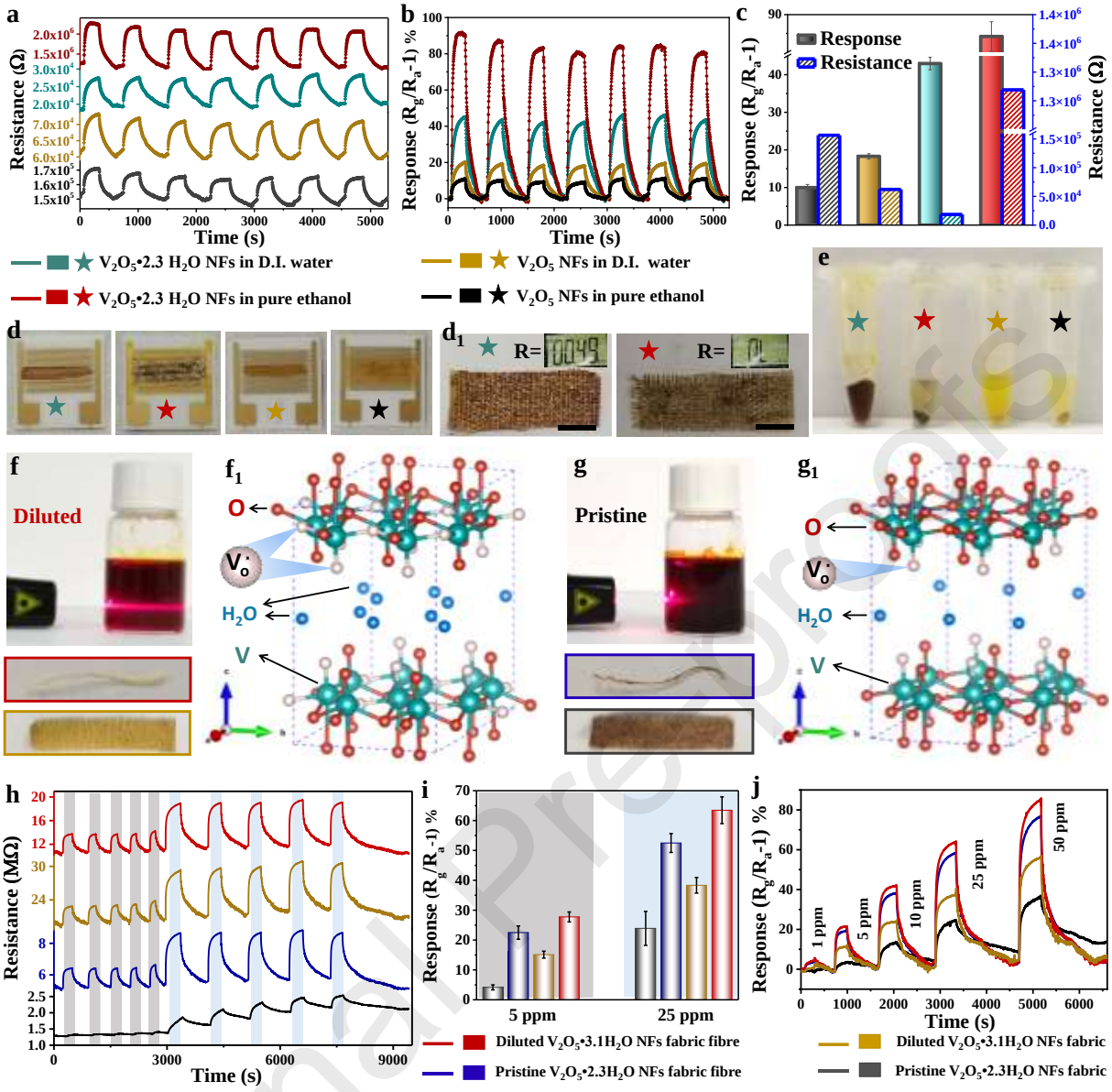

Fig. 2. The NH_3 sensing comparison between freeze-dried and annealed $V_2O_5 \cdot 2.3H_2O$ NFs powder being dispersed in D.I. water and pure ethanol, respectively. (a) The real-time resistance and (b) sensing curves to 10 ppm NH_3, and corresponding (c) histogram of baseline resistance and response value. (e) The photograph of above four dispersions and (d) integrated interdigital electrode. (d_1) The freeze-dried $V_2O_5 \cdot 2.3H_2O$ NFs dispersed in D.I. water and pure ethanol were integrated onto the fabric, respectively. The scale bars in (d_1) are 0.5 cm. The photographs and structures of (f-f_1) diluted and (g-g_1) pristine $V_2O_5 \cdot nH_2O$ NFs inks. The "Tyndall effect" of diluted $V_2O_5 \cdot 3.1H_2O$ NFs ink irradiated by red light (λ = 638 nm). The comparison on NH_3 sensing performance between diluted and pristine $V_2O_5 \cdot nH_2O$ NFs inks integrated on fabric and the fabric fiber, respectively. (h) The real-time resistance curves and (i) the summarized responses. (j) The response curves to various NH_3 concentration. The RH of (a-b, h-j) is at ~ 22%.

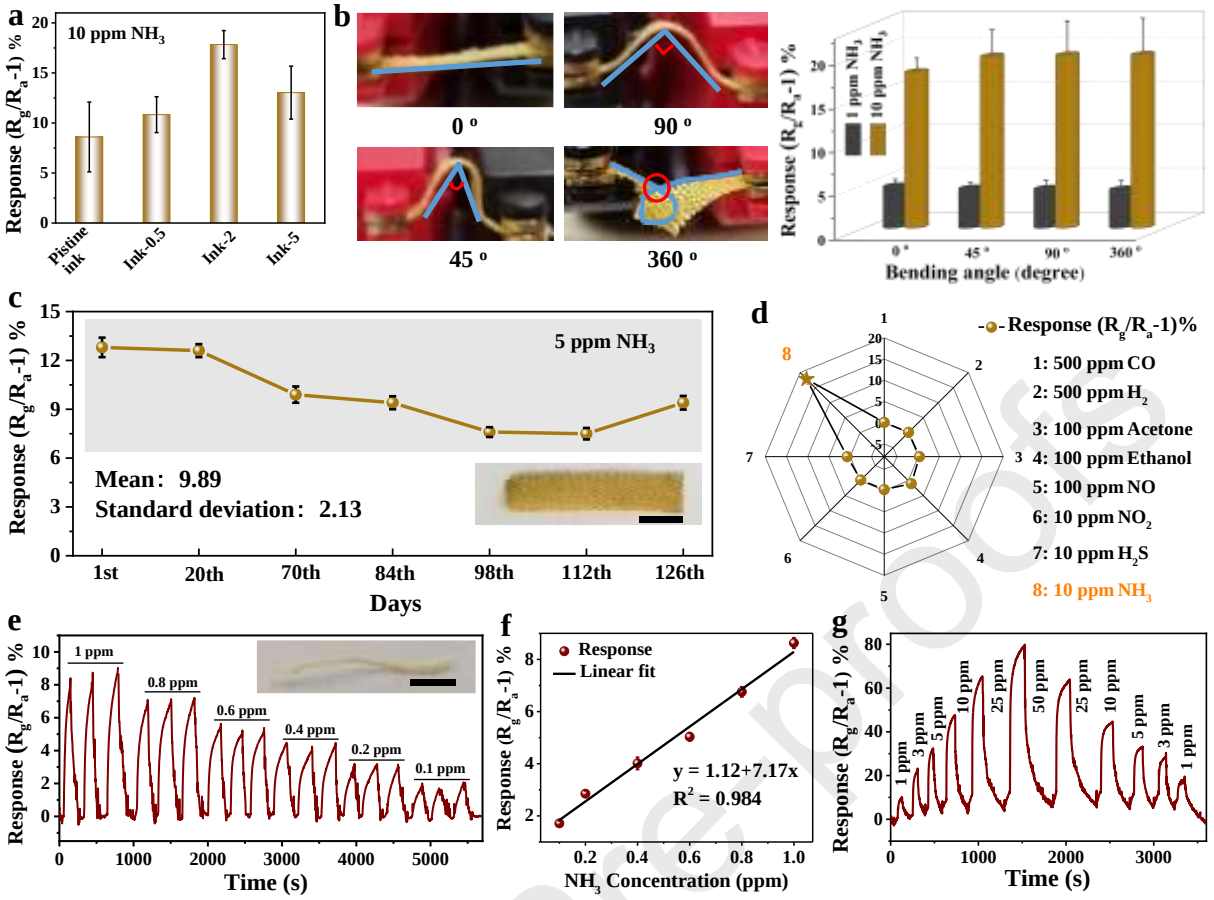

Fig. 3. The systematic NH_3 sensing evaluation of $V_2O_5 \cdot nH_2O$ NFs ink integrated over fabrics: (a) The dilution-dependent sensing response of $V_2O_5 \cdot nH_2O$ NFs ink, (b) the $V_2O_5 \cdot 3.1H_2O$ NFs fabric under various bending angle and their corresponding sensing responses, (c) the long-term stability and (d) selectivity of diluted $V_2O_5 \cdot 3.1H_2O$ NFs fabric. The NH_3 sensing evaluation of $V_2O_5 \cdot 3.1H_2O$ NFs fabric fiber: (e) The response curve to 0.1-1 ppm NH_3, (f) the relationship between sensing responses and NH_3 concentrations, (g) the response curve to various NH_3 concentrations. The scale bars in (c) and (e) are 0.5 cm. The RH of (a-b, d, e-g) is at ~ 19% and RH of (c) is at ~ 19%-57%.

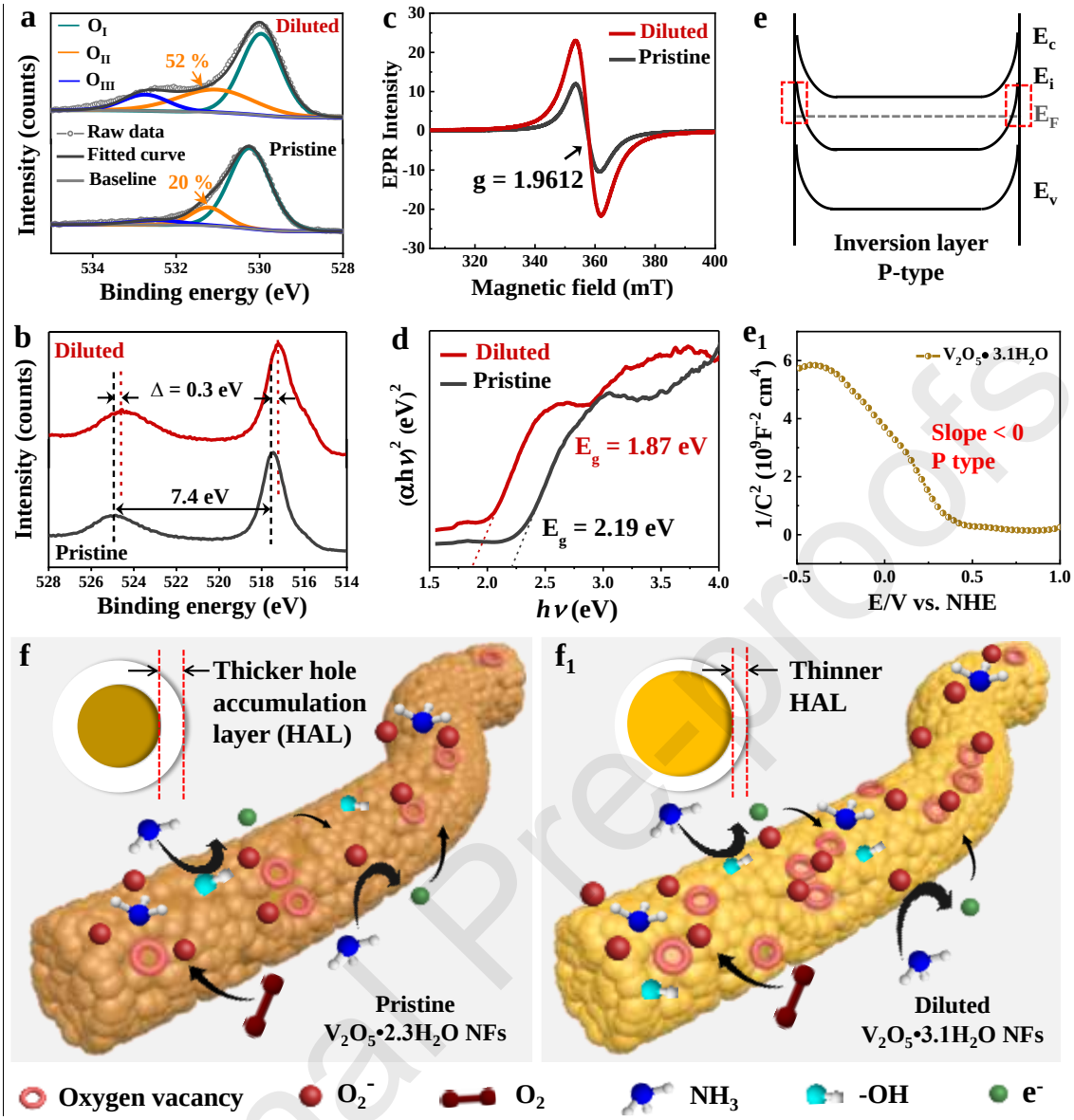

Fig. 4. The various characterizations on oxygen vacancy of pristine $V_2O_5 \cdot 2.3H_2O$ NFs and diluted $V_2O_5 \cdot 3.1H_2O$ NFs. High-resolution XPS spectra are related to (a) O 1s and (b) V 2p, (c) EPR spectra and (d) plots of $(ahv)^2$ vs photon energy (hv). The schematic energy-band variation of $V_2O_5 \cdot nH_2O$ NFs. (e) An inversion layer marked with red rectangle and p-type surface conductivity. (e_1) The Mott-Schottky plot of $V_2O_5 \cdot 3.1H_2O$ NFs. The NH_3 sensing mechanism diagrams of (f) pristine $V_2O_5 \cdot 2.3H_2O$ NFs and (f_1) diluted $V_2O_5 \cdot 3.1H_2O$ NFs.

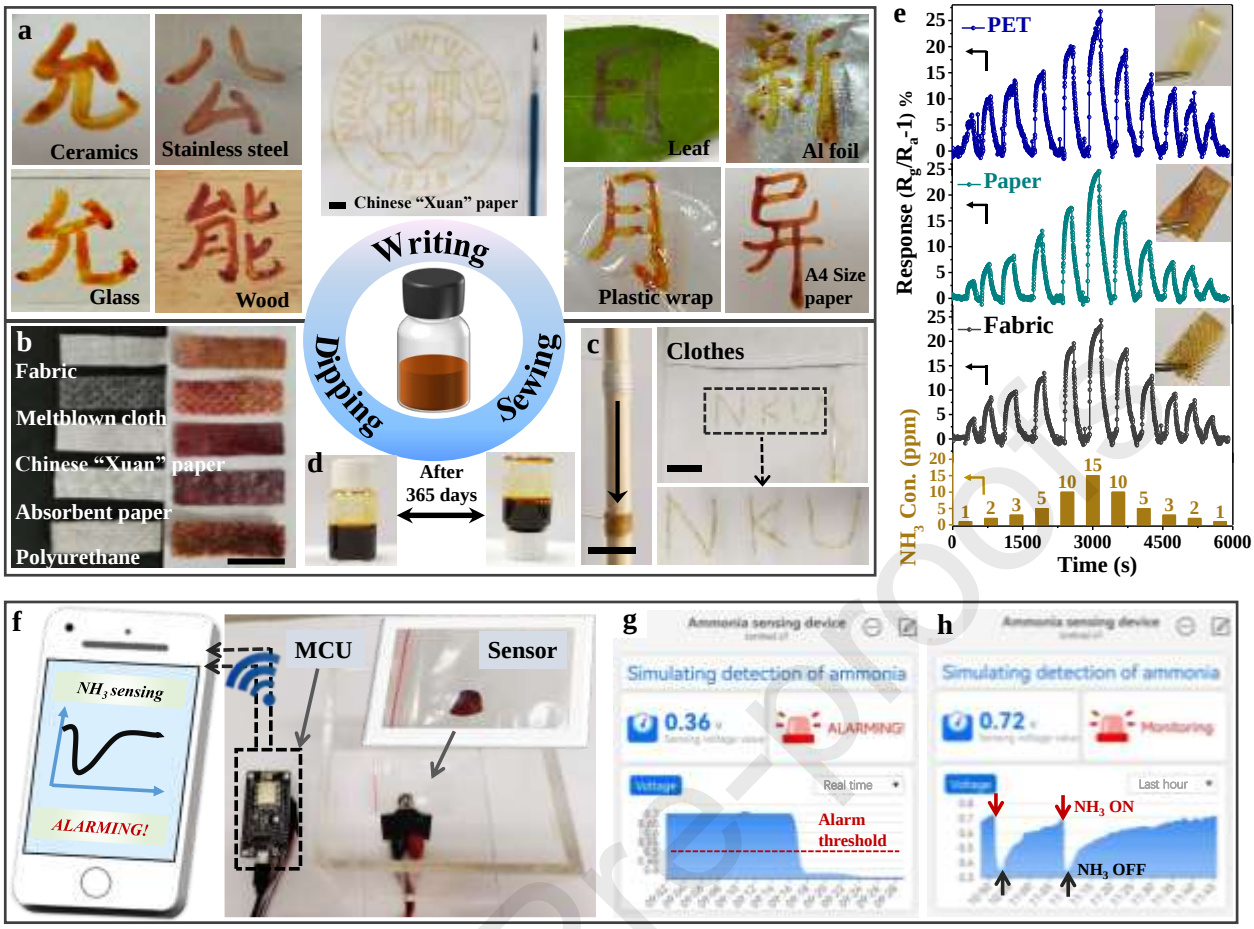

Fig. 5. The universal substrates-tolerant and multi means-integratable NH_3 sensing. (a) The $V_2O_5 \cdot 2.3H_2O$ NFs ink for drawing the school badge and the motto of Nankai University onto hard and flexible substrates. (b) The pristine $V_2O_5 \cdot 2.3H_2O$ ink was evenly integrated onto various flexible substrates as examples. (c) The diluted $V_2O_5 \cdot 3.1H_2O$ NFs ink integrated fabric fiber for sewing patterns into clothes. (d) The photographs of $V_2O_5 \cdot 3.1H_2O$ NFs ink after storing 365 days. (e) The NH_3 sensing of diluted $V_2O_5 \cdot 3.1H_2O$ NFs ink integrated on flexible substrates with PET, Chinese "Xuan" paper and fabric as examples, and "Con." in the ordinate represents concentration. The scale bars in (a, b, c) are all 1 cm. (f) Simulated detection of NH_3 were conducted by intergrating the $V_2O_5 \cdot 3.1H_2O$ NFs ink onto sample bag and communicating with a smartphone. (g) Smartphone reading the real-time sensing parameters and the records of alarming to 10 ppm NH_3 and (h) the historical measurements. The RH of (e) is at ~ 22%.

557 **Table 1.** Comparison of various NH_3 sensing materials in both presenting forms and NH_3
558 sensing.

Material type	Materials	Presenting forms	Substrates	Mechanical flexibility	Integrating means	WT [a]	Response@Con. [c]	T_{res}/T_{rec} time (s) @Con. [c]	LOD [h] (ppm)	Refs. [k]
SMOs based NH_3 sensing materials	Co-Fe_2O_3	powder	ceramic tube	No	spin-coating combined with calcination	275 °C	275% [d]@10 ppm	7.2/5.4@10 ppm	0.01 [i]	[42]
	MoO_3 nanorods	powder	glass	No	spin-coating by mixing with solvent	200 °C	36% [d]@5 ppm	230/267@5 ppm	~5 [i]	[8]
	WO_3@SnO_2 Core shell nanosheet	thin film	MEMS	No	dripping-coating by mixing with solvent	200 °C	1.5 [e]@15 ppm	62/42@15 ppm	5 [i]	[43]
	Ni-doped In_2O_3 nanostructure	powder	ceramic tube	No	coating by mixing with solvent	140 °C	2732 [e]@50 ppm	23/10@50 ppm	~1 [i]	[9]
	MXene/CuO composite.	solution	epoxy	Yes	spraying	RT	24.8 [f] @100 ppm	43/26@100 ppm	~1 [i]	[41]
	MXene/V_2O_5/$CuWO_4$	precipitate	alumina sheet with interdigitated gold electrode	No	coating	RT	53.5 [f] @51 ppm	1.6/4@51 ppm	1 [i] 0.3 [j]	[44]
	$V_2O_5 \cdot nH_2O$ NFs	**ink**	**ceramics, stainless steel, glass, wood, paper, leaf, Al foil, plastic wrap, fabric and polyurethane**	**Yes**	**dripping, writing, dipping and sewing**	**RT** [b]	**~4.2% [g]@1 ppm**	**75/36@1 ppm**	~ 0.1 [i]	**This work**
Carbon based NH_3 sensing	PANI/MWCNTs	-	polypropylene fabric	Yes	spray-coating and chemical polymerization	RT	61.54% [g]@20 ppm	9/30@20 ppm	0.2 [j]	[45]

materials										
	PEDOT:PSS nanowires	aqueous suspension	PET	Yes	spin-coating	RT	~2.2% [g)]@6 ppm	96/318@6 ppm	0.1 [j)]	[19]
	PSS-PANI/PVDF	-	PVDF membrane	Yes	in-situ polymerization	RT	70% [g)]@1 ppm	160/400@1 ppm	~ 0.1 [i)]	[46]
	Pt-NDs/PPy-nanolayer@CNTs	powder	filter paper	Yes	coating by mixing with solvent	RT	~40% [g)] @50 ppm	2/~10@2 v/v%	~0.005 [j)]	[20]
	PANI/$NiCo_2O_4$	powder	gelatin film	Yes	spin-coating	RT	4.67 [f)]@20 ppm	22/62@20 ppm	~ 0.5 [i)]	[47]
	PANI/MXene	solution	epoxy	Yes	dripping	RT	27% [g)]@5 ppm	27/5@5 ppm	~ 0.3 [i)]	[48]
	SnPx/rGO	powder	interdigitated electrodes	No	dripping	RT	117.5% [d)] to 40 ppm	126/306@10 ppm	0.0436 [j)]	[49]

[a)] Working temperature, [b)] Room temperature, [c)] Concentration, [d)] Calculated by (R_a/R_g-1)*100%, [e)] Calculated by R_a/R_g, [f)] Calculated by R_g/R_a, [g)] Calculated by (R_g/R_a-1)*100%, [h)] Limit of Detection, [i)] Experimental measurements, [j)] Theoretical calculation, [k)] References.

Declaration of interests

☒ The authors declare that they have no known competing financial interests or personal relationships that could have appeared to influence the work reported in this paper.

☐The authors declare the following financial interests/personal relationships which may be considered as potential competing interests:

Graphical Abstracts

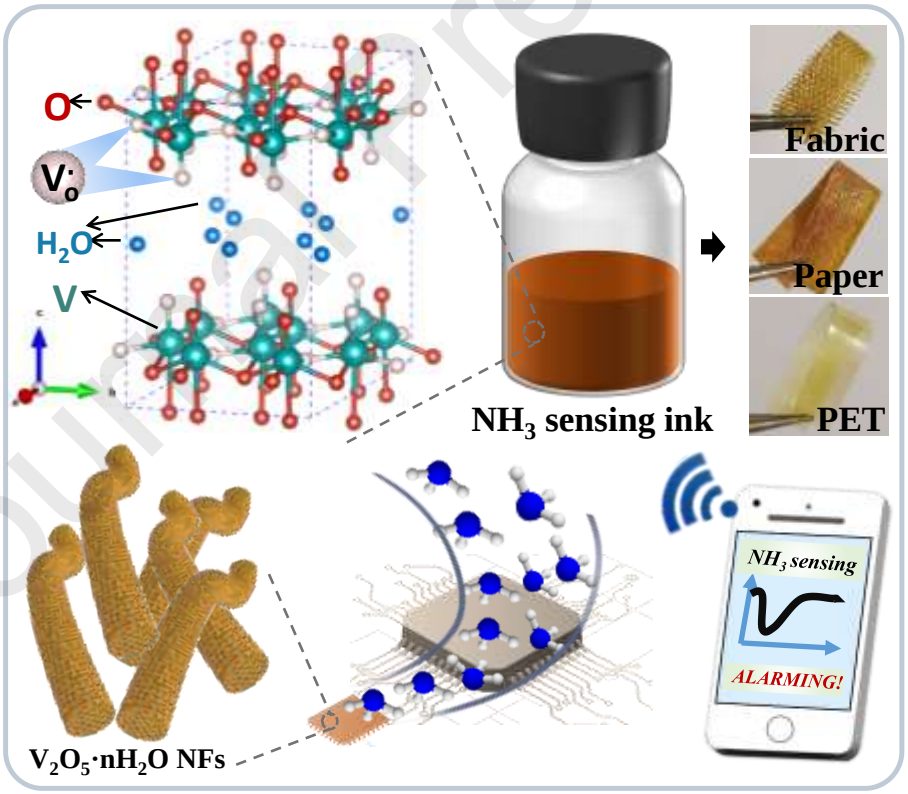

Highlights

1. The excellent dispersed and stable $V_2O_5{\cdot}3.1H_2O$ nanofibers ink has been developed.

582 2. The ink toward universal substrates-tolerant and multi means-integratable NH_3 sensing.

583 3. The oxygen vacancy governed NH_3 sensing mechanism is rationally interpreted.

584 4. Simulation on detecting NH_3 is conducted with reliable sensing response.

585